Growth of WS_2 Nanotubes Phases

A. Rothschild,[†] J. Sloan,[‡] and R. Tenne*,[†]

Contribution from the Department of Materials and Interfaces, Weizmann Institute of Science, Rehovot 76100, Israel, and Inorganic Chemistry Laboratory, University of Oxford, South Parks Road, Oxford OX1 3QR, UK

Received November 24, 1999

Abstract: Recently, a method to produce bulk quantities of pure multiwall WS_2 nanotubes, which could reach several microns in length, has been developed. A detailed study of the growth mechanism of these WS_2 nanotubes has been undertaken, which is reported hereby. A series of experiments were conducted to define the key parameters, which determine the shape of the WS_2 nanotubes. An alternative approach for the synthesis of WS_2 nanotubes, starting from long WO_{3-x} nanowhiskers, which can be extended for the synthesis of other nanotubes, is described as well.

I. Introduction

The discovery of carbon nanotubes in 1991[1] has generated intense experimental and theoretical interest over the past few years because of their unusual geometry and physical properties. Besides the original carbon structure, similar inorganic structures have also emerged: BN,[2] V_2O_5,[3] MoS_2,[4−7] WS_2[6,8,9], etc. The reason for such an analogy between the pure carbon and inorganic structures is based on the fact that they all stem from lamellar (2D) compounds. Consequently, a lot of effort has been recently devoted to the study of nanotubes from other new related materials.

The case of the layered transition-metal dichalcogenides (WS_2 and MoS_2) was the first example of such an analogy. Indeed, in 1992, IF (inorganic fullerene-like) structures and nanotubes of WS_2 were reported,[9] followed shortly by similar results on MoS_2[10] and the respective selenides.[11] However, it is noteworthy to underline that the samples contained minute amounts of IF particles. Instead, most of the samples consisted of WS_2 platelets (2H-WS_2). The nanotubes were relatively rare and constituted even a smaller fraction of the total composition. Besides this statistical fact, the reproducibility of the nanotubes growth was rather poor. Recently, a short communication describing the growth of a pure phase of WS_2 nanotubes has been published.[12]

In the present work, the strategy and the parameters that control the synthesis of WS_2 nanotubes are presented and the growth mechanism is discussed. A complementary synthetic method of WS_2 and WSe_2 nanotube phases is demonstrated hereby, too.

The procedure chosen for the formation of WS_2 nanotubes is an extension of a synthetic process for IF-WS_2 particles.[13] Indeed, the present process could also be described as the conversion of tungsten oxide particles into WS_2 nanotubes by reacting the oxide in a reducing (H_2) and sulfidizing atmosphere (H_2S) at elevated temperature (840 °C). However, for orientating the growth to a phase composed in its greatest majority of WS_2 nanotubes, an asymmetric tungsten oxide precursor, which contains already the "future shape" of a nanotube, was used instead of the quasispherical WO_3 particles. The method for providing such needlelike morphology is based on the evaporation of a hot tungsten filament in the presence of water vapor. Preliminary attempts to produce tungsten oxide nanoparticles have given mixtures of spherical particles.[14] An optimization of this procedure was performed to get a single phase of needlelike particles. Once this goal was reached (see section III.1), the needlelike particles were employed as precursors for the synthesis of the WS_2 nanotubes (see section III.2).

II. Experimental Section

II.1. Synthesis of the WO_{3-x} Particles. Tungsten suboxide particles (WO_{3-x}) were produced by heating a tungsten filament (model ME11 from the R. D. Mathis company) in the presence of water vapor inside a vacuum chamber. The following procedure was used: once the vacuum in the bell-jar had reached a value of 10^{-4} Torr, the filament was heated for a few minutes to remove the superficial oxide layer. Water vapor was then allowed to diffuse into the vacuum chamber through an inlet, until the desired pressure was reached. The filament was heated to around 1600 ± 20 °C, while the pressure in the chamber

* Author of correspondence e-mail: reshef.tenne@weizmann.ac.il.
† Weizmann Institute of Science.
‡ University of Oxford.

(1) Iijima, S. *Nature* **1991**, *56*, 354.
(2) (a) Chopra, N. G.; Luyken, R. J.; Cherrey, K.; Crespi, V. H.; Cohen, M. L.; Louie, S. G.; Zettl, A. *Science* **1995**, *269*, 966. (b) Stephan, O.; Ajayan, P. M.; Colliex, C.; Redlich, Ph.; Lambert, J. M.; Bernier, P.; Lefin, P. *Science* **1994**, *266*, 1683.
(3) Ajayan, P. M.; Stephan, O.; Redlich, Ph.; Colliex, C. *Nature* **1995**, *375*, 564.
(4) Remskar, M.; Skraba, Z.; Cleton, F.; Sanjines, R.; Levy, F. *Appl. Phys. Lett*. **1996**, *69*, 351.
(5) Zelenski, C. M.; Dorhout, P. K. *J. Am. Chem. Soc*. **1998**, *120*, 734.
(6) Remskar, M.; Skraba, Z.; Ballif, C.; Sanjines, R.; Levy, F. *Surf. Sci.* **1999**, *435*, 637.
(7) Feldman, Y.; Wasserman, E.; Srolovitz, D.; Tenne, R. *Science* **1995**, *267*, 222.
(8) (a) Remskar, M.; Skraba, Z.; Regula, M.; Ballif, C.; Sanjines, R.; Levy, F. *Adv. Mater*. **1998**, *10*, 246. (b) Remskar, M.; Skraba, Z. *Appl. Phys. Lett*. **1999**, *74*, 3633.
(9) Tenne, R.; Margulis, L.; Genut, M.; Hodes, G. *Nature* **1992**, *360*, 444.
(10) Margulis, L.; Salitra, G.; Talianker, M.; Tenne, R. *Nature* **1993**, *365*, 113.
(11) Hershfinkel, M.; Gheber, L. A.; Volterra, V.; Hutchison, J. L.; Margulis, L.; Tenne, R. *J. Am. Chem. Soc*. **1994**, *116*, 1914.
(12) Rothschild, A.; Frey, G. L.; Homyonfer, M.; Rappaport, M.; Tenne, R. *Mater. Res. Innoat.* **1999**, *3*, 145.
(13) (a) Feldman, Y.; Frey, G. L.; Homyonfer, M.; Lyakhovitskaya, V.; Margulis, L.; Cohen, H.; Hodes, G.; Hutchison, J. L.; Tenne, R. *J. Am. Chem. Soc.* **1996**, *118*, 5362. (b) Feldman, Y.; Lyakhovitskaya, V.; Tenne, R. *J. Am. Chem. Soc.* **1998**, *120*, 4176.
(14) Homyonfer, M.; Alperson, B.; Rosenberg, Y.; Sapir, L.; Cohen, S. R.; Hodes, G.; Tenne, R. *J. Am. Chem. Soc.* **1997**, *119*, 2693.

10.1021/ja994118v CCC: $19.00
Published on Web 05/13/2000

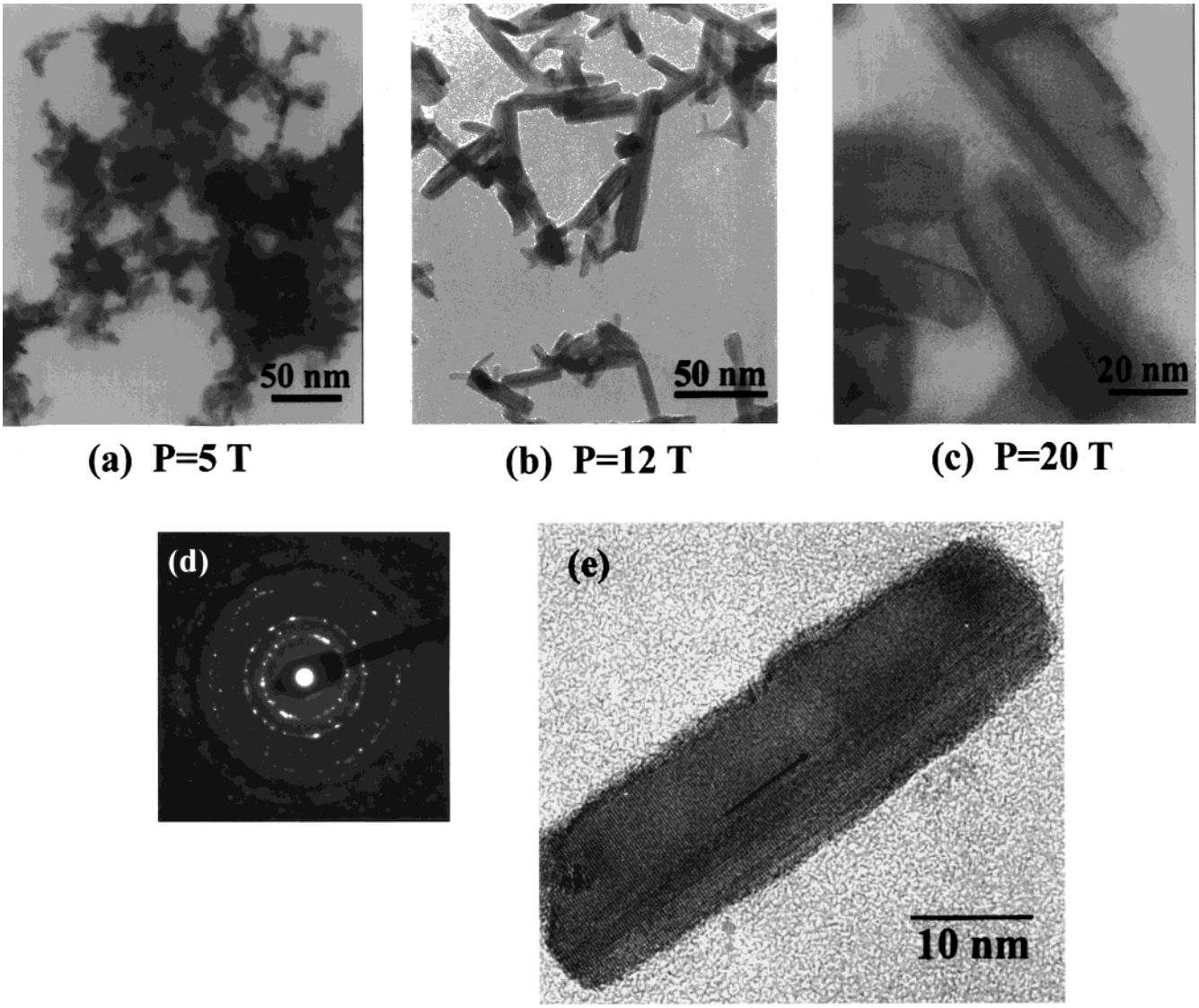

Figure 1. TEM micrographs and the corresponding ED patterns of tungsten oxide particles WO_{3-x} synthesized at different water vapor pressure: (a) $P_{H_2O} = 5$ Torr; (b) $P_{H_2O} = 12$ Torr; and (c) $P_{H_2O} = 20$ Torr. (d) ED of the WO_{3-x} particles synthesized at $P_{H_2O} = 12$ Torr and $P_{H_2O} = 20$ Torr. (e) Enlargement of one whisker produced at $P_{H_2O} = 12$ Torr. Defects along the whisker axis are indicated.

was maintained constant during the evaporation process (a few Torr). After a few minutes of evaporation, a blue powder condensed on the bell-jar walls. The accrued powder consisted of needlelike WO_{3-x} particles (ca. 50 nm in length and 15 nm in diameter) under a specific water vapor pressure (vide infra).

$NiCl_2$ or $CoCl_2$ (2×10^{-3} M) salts were dissolved in the water reservoir before each evaporation. The nanoparticles produced in the presence of the transition-metal salt appeared to be more crystalline than those obtained without the addition of a salt, as shown by ED.

II.2. Synthesis of the WS_2 Nanotubes Starting from the WO_{3-x} Nanoparticles. The synthesis of the WS_2 nanotubes starting from the needlelike WO_{3-x} particles was done in a reactor similar to the one used for the synthesis of IF-WS_2 particles.[13] The principle of the synthesis is based on a solid−gas reaction, where a small quantity (5 mg) of WO_{3-x} particles (solid) is heated to 840 °C under the flow of H_2/N_2 (forming gas) + H_2S gas mixture. To avoid cross-contamination between the different runs and minimize memory effects, which can be attributed to the decomposition of H_2S and deposition of sulfur on the cold walls of the reactor, flushing of the reactor (10 min) with N_2 gas flow was performed after each synthesis.

Samples were studied using a scanning electron microscope (SEM) Philips XL30-ESEM FEG instrument, a transmission electron microscope (TEM) Philips CM 120 (120 keV), and an X-ray diffraction instrument (Rigaku Rotaflex RU-200B) having a Cu Kα anode. The electron diffraction (ED) patterns were obtained on a high-resolution transmission electron microscope (HRTEM) JEM-4000EX operated at 400 kV. Ring patterns from TiCl were used as a calibration reference standard for the ED patterns. The accuracy of the *d* spacings is estimated at ±0.005 nm.

III. Results

III.1. Synthesis of Tungsten Oxide Needlelike Particles (Stage I). Three different values of water vapor pressure were selected: $P_{H_2O} = 5$, 12, and 20 Torr, the latter corresponding to the thermodynamic limit of the water vapor pressure at room temperature (22 °C). The texture of all the batches appeared to be more or less the same after a few minutes of evaporation. However, a variation in the color of the powder, which was collected on the walls of the bell-jar, was noticed. A color range, which goes from dark blue for $P_{H_2O} = 5$ Torr to light blue for $P_{H_2O} = 20$ Torr was observed.

Apparently, the water vapor pressure in the chamber influences the morphology and the stoichiometry of the nanoparticles obtained by evaporation. For a low value ($P_{H_2O} = 5$ Torr), the oxide nanoparticles did not have a well-defined morphology (Figure 1a). The ED pattern confirms that the powder is completely amorphous (not shown here). When the pressure was increased ($P_{H_2O} = 12$ Torr), the nanoparticles presented a

Table 1. Comparative *d* Spacing Data between the Needlelike Precursors and the Tetragonal $WO_{2.9}$ Reported by Glemser[15a,a]

oxide precursors		tetragonal $WO_{2.9}$[15a]		
I_{rel}	d_{hkl} (Å)	I_{rel}	d_{hkl} (Å)	hkl
100	3.752	100	3.74	110
20	3.206	20	3.10	101
80	2.640	80	2.65	200
30	2.184	30	2.20	201
		10	2.02	211
30	1.878	30	1.88	220
10	1.703	10	1.78	300
60	1.558	60	1.67	310
50	1.153	50	1.53	311
		10	1.33	222
		10	1.25	330
		10	1.17	322

[a] the d_{hkl} spacings were obtained from the ED ring pattern of the oxide particles. A TiCl pattern was used as a standard reference.

cylindrical shape and were crystalline. A typical batch is shown in Figure 1b, where the dimensions of the whiskers are typically around 50 nm in length and 15 nm in diameter. For the thermodynamic limit of the water pressure at room temperature (P_{H_2O} = 20 Torr), a growth in both directions (along the nanoparticle long axis and perpendicular to it) led to the formation of needlelike particles with a much smaller aspect ratio and steps perpendicular to the long axis. The whiskers are crystalline as could be evidenced from the ED pattern, which is similar to the one observed for the particles produced at 12 Torr (see Figure 1c).

The stoichiometry of the particles could not be easily assigned by XRD for several reasons. First, most of the samples were not sufficiently crystalline for generating well-defined peaks in the spectrum. Moreover, several nonstoichiometric tungsten oxide phases have been reported in the literature and all of them exhibit very similar patterns. Consequently, assigning the stoichiometry of the concerned phase accurately from the XRD data was rather difficult. The measurement by electron diffraction of a bundle of individual needlelike crystals was more informative in this case. The values of the d_{hkl} spacings were calculated for the crystalline whiskers synthesized at P_{H_2O} = 12 and 20 Torr. Both sets of whiskers can be interpreted as having an average substructure similar to that of the reported tetragonal phase $W_{20}O_{58}$ ($WO_{2.9}$) originally described by Glemser et al.[15a] (Table 1). The needles can be described according to a substructure of WO_3 interspersed with defects attributable to random crystallographic shear planes occurring either parallel to the needle axis or, alternatively, at some angle to the beam direction as the needles are viewed in the HRTEM. Further evidence of the randomness of the defects occurring in the needles is given by the prominent diffuse streaking that is often observed in ED patterns obtained from these needles[15b] (see also Figure 1d). An example of a needlelike particle containing random defects is shown in Figure 1e. It is noteworthy to underline that, whatever the pressure inside the chamber, the batches appeared to be homogeneous in their morphology, providing needlelike particles of relatively constant oxide stoichiometry for a given preparation.

Hereafter, a detailed study of the conditions required for the whisker's growth was undertaken. The role of the water in this process was examined first.

III.1.a. The Role of Water. To get an idea of the role of water in the oxidation of the tungsten filament, evaporations were performed with oxygen instead of water vapor in the chamber. Indeed, oxidation of the tungsten filament could be performed either with water vapor according to eq 1 or with pure oxygen (eq 2), both reactions being exothermic in the conditions of the present measurements (temperature of the filament, 1600 ± 20 °C; pressure in the chamber maintained at 12 Torr). The free energies of the reactions were calculated using the data given in ref 16 for STP (standard) conditions.

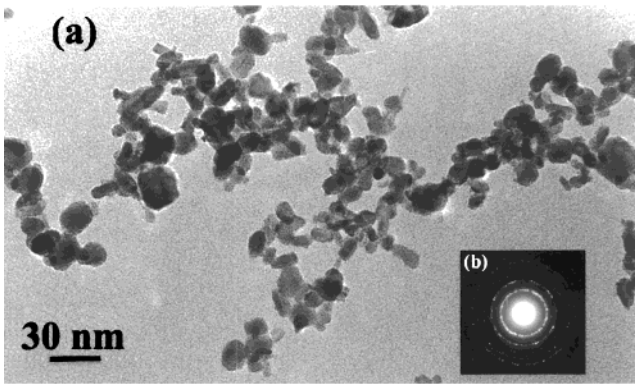

Figure 2. (a) TEM micrograph of tungsten oxide particles WO_{3-x} synthesized at P_{O_2} = 6 Torr and (b) the corresponding ED pattern of the WO_{3-x} particles synthesized at P_{O_2} = 6 Torr.

$$W\,(s) + 3H_2O\,(g) \rightarrow WO_3\,(s) + 3H_2\,(g) \qquad (\Delta G_{(1873\ K\ and\ P=12\ T)} = -21\ kJ\ mol^{-1})^{16} \quad (1)$$

$$W\,(s) + {}^3/_2O_2(g) \rightarrow WO_3(s) \qquad (\Delta G_{(1873\ K\ and\ P=12\ T)} = -150.5\ kJ\ mol^{-1})^{16} \quad (2)$$

To perform the evaporation with the same quantity of oxygen as for the one performed in the presence of water vapor, the oxygen pressure was maintained at P_{O_2} = 6 Torr compared to P_{H_2O} = 12 Torr ($n_{O_2} = {}^1/_2 n_{H_2O}$). The resultant particles were 100% spherical or faceted, typically 5 to 30 nm in diameter (see Figure 2). The color of the powder was light blue, which can be ascribed to a slight reduction of the powder by traces of water still present in the vacuum chamber. When the oxygen pressure was decreased, light blue phases of spherical or faceted nanoparticles were observed as well.

The absence of needlelike particles in the presence of oxygen in the chamber is indicative of the role played by hydrogen in generating an asymmetric growth of the nanoparticles (see eqs 1 and 2).

These findings allude to the fact that the needles growth consists of a two-step process occurring simultaneously on the hot filament surface. The first step is the oxidation of the tungsten filament, which leads to the formation of WO_3 particles. In the next step, reduction of these particles results in the formation of WO_{3-x} needlelike particles (eq 3).

$$WO_3\,(s) + H_2\,(g) \rightarrow WO_{3-x}\,(g) + xH_2O\,(g) + (1-x)H_2\,(g) \quad (3)$$

It is important to note that the direct reaction between water vapor and the W filament is not the only plausible oxidation route. Indeed two pathways could be contemplated for the oxidation of W with water. The first one corresponds to the direct reaction of water molecules with W atoms (eq 1).

(15) (a) Glemser, O.; Weidelt, J.; Freund, F. *Z. Anorg. Allg. Chem*. **1964**, *332*, 299. (b) Sloan, J.; Hutchison, J. L.; Tenne, R.; Feldman, Y.; Tsirlina, T.; Homyonfer, M. *J. Solid State Chem.* **1999**, *144*, 100.

(16) *Handbook of Chemistry and Physics*, 69th ed.; Weast, R. C., Editor-in-Chief; CRC Press, Inc.: Boca-Raton, FL, 1988−1989; pp D50−93.

Table 2. Influence of an Auxiliary Gas on the Morphology of the Particles[a]

(a) Argon

P_{H_2O} (Torr)	P_{Ar} (Torr)	P_{H_2O}/P_{Ar}	P_{H_2O}/P_{Tot}	P_{Tot} (Torr)	morphology of the particles
5	2.5	2	0.66	7.5	N-thin ($l \cong 50$ nm and $D \cong 15$ nm) + amorphous material
5	5	1	0.5	10	N-thin ($l \cong 50$ nm and $D \cong 15$ nm)
5	20	0.25	0.2	25	N-thin ($l \cong 90$ nm and $D \cong 15$ nm) + N-thick ($l \cong 90$ nm and $D \cong 30$ nm)
5	40	0.125	0.11	45	N-thin ($l \cong 110$ nm and $D \cong 15$ nm) + N-thick ($l \cong 130$ nm and $D \cong 30$ nm) + ⟨F−N⟩
12	12	1	0.5	24	N-thin ($l \cong 90$ nm and $D \cong 15$ nm) + N-thick ($l \cong 90$ nm and $D \cong 30$ nm)
12	48	0.25	0.2	60	<S−F> ($D \cong 25$ nm) + few N-thick ($l \cong 50-300$ nm and $D \cong 35-180$ nm)

(b) Hydrogen

P_{H_2O} (Torr)	P_{H_2} (Torr)	P_{H_2O}/P_{H_2}	P_{H_2O}/P_{Tot}	P_{Tot} (Torr)	morphology of the particles
5	5	1	0.5	10	N-thin
5	20	0.25	0.2	25	no evaporation
12	1	12	≅12	13	N-thin with more defects along the needle's axis
12	5	2.4	0.7	17	N-thin with more defects along the needle's axis

[a] N denotes particles with a needlelike morphology. *l* denotes length of the particles. *D* denotes diameter of the particles. ⟨F−N⟩ denotes particles with a morphology of between faceted and needlelike. ⟨S−F⟩ denotes particles between spherical and faceted.

Alternatively, partial water decomposition (see eq 4) leads to the oxidation of the hot tungsten filament by liberated oxygen.

$$H_2O\,(g) \rightarrow {}^1/_2O_2\,(g) + H_2\,(g)(\Delta G_{(1873\ K\ and\ P=12\ T)} = +33.9\ kJ\ mol^{-1})^{16} \quad (4)$$

Regardless of whether the direct or indirect mechanism is correct, H_2 is a resultant product of both reactions. It is therefore believed that hydrogen is involved in the production of needlelike particles as opposed to the spherical ones, which are obtained in the absence of hydrogen in the chamber.

III.1.b. Attempts to Increase the Size of the Needlelike Particles. In this series of experiments, the effect of different gases on the growth mode of the nanoparticles was examined. Since thermodynamics dictates that water vapor pressure cannot exceed 20 Torr at room temperature, addition of different gases (Ar or H_2) was attempted. Argon and hydrogen have a similar mean free path in the prevalent conditions ($\lambda_{Ar} = 4.73\ 10^{-5}$ m and $\lambda_{H_2} = 8.81 \times 10^{-5}$ m at 20 °C and 1 Torr);[16] however, hydrogen is directly implicated in the tungsten oxide whisker growth, while argon is chemically inert. The two sets of experiments were therefore used as a tool for underpinning the importance of the chemical nature of the gas in the process. Indeed, in addition to water (partial vapor pressure of $P_{H_2O} =$ 5 and 12 Torr), argon was introduced first into the chamber in different partial pressures. Note that for $P_{H_2O} = 12$ Torr, oxide nanowhiskers are formed, while a partial pressure of 5 Torr of water leads to the formation of amorphous tungsten oxide nanoparticles.

The results obtained with the addition of argon in the chamber are summarized in Table 2a. It appears that needlelike particles are formed under 5 Torr of water vapor pressure complemented by 5 Torr of argon. This is rather surprising since the same partial pressure of water alone led to the formation of an amorphous material (see Figure 1a). Keeping the partial pressure of water constant, the argon pressure was elevated step by step, until a total pressure of 60 Torr was reached. The morphology of the whiskers begins to change already around 25 Torr, whence a second growth direction, perpendicular to the whisker's main axis, starts to evolve. Here, a stepwise growth mode is apparent, with new terraces added to the incipient whisker outer perimeter. This kind of "thick whisker" growth mode is similar to the results obtained for $P_{H_2O} = 20$ Torr (see Figure 1c). A mixture of thick whiskers and faceted particles could be observed above a total pressure of 25 Torr. Finally, when the total pressure had reached 60 Torr, essentially spherical or faceted particles (25 nm in diameter) and some remaining needlelike particles with steps (50−300 nm long and 35−180 nm thick) were present in the sample.

Accordingly, to have a pure phase of needlelike tungsten oxide particles, the total pressure has to be kept in the range 10−25 Torr, with at least 5 Torr of water vapor pressure.

The same procedure was repeated with an additional pressure of hydrogen instead of argon (Table 2b). As can be seen, the partial pressure of hydrogen also influences the morphology of the tungsten oxide particles. Indeed, for a total pressure of 25 Torr ($P_{H_2O} = 5$ Torr), no evaporation of the metal could be detected whatsoever, although for the same total pressure with argon instead of hydrogen, whiskers were formed (see Table 2a). This result emphasizes the fact that the nature of the gas has an important influence on the morphology of the particles. According to eq 1, addition of hydrogen into the vacuum chamber shifts the reaction to the left, thereby blocking the formation of WO_3 and its subsequent sublimation (at 1600 °C). When the ratio of the partial vapor pressures $P_{H_2O}/P_{H_2} \geq 0.5$, the needlelike morphology is nevertheless conserved (see Table 2b). In this case, the reducing power of hydrogen is not strong enough to halt the formation of WO_3 nanoparticles, but is sufficient to promote the growth of the needlelike particles. Note also that, under these conditions ($P_{H_2O} = 12$ Torr and $P_{H_2} =$ 1 or 5 Torr), a much larger density of random defects was observed in the oxide needles as compared to those produced by evaporation performed in the absence of hydrogen (Table 2b).

Accordingly, when a reactive gas such as hydrogen is introduced into the chamber, either directly (as H_2) or indirectly (as H_2O), both the reactive gas pressure (P_{gas}) and the total pressure in the chamber (P_{Tot}) have to be considered.

Unfortunately, no improvement in the aspect ratio and the length of the needles was observed in all the sets of experiments described in this section.

III.1.c. Attempts to Increase the Needlelike Particle Length via High-Temperature Reaction (Stage II). Since hydrogen was found to be indispensable for the growth of the needles, an alternative procedure for promoting their growth under more controllable conditions was pursued. The basic idea was to promote the uniaxial growth of the short tungsten suboxide needles obtained in stage I under very low hydrogen gas concentration. For that purpose, the needles were placed in a reactor operating at around 840 °C in a flow of (H_2/N_2) gas mixture where the concentration of hydrogen was progressively

Table 3. Influence of the Hydrogen Concentration on the Morphology of the Particles[a]

(a) Mixture of 1% H_2/99% N_2

P_{H_2O} (Torr)	flow 1% H_2/99% N_2 (cm^3 min^{-1})	morphology of the particles
5	110	L_{ox-t} and L_{ox-T} (>1 μm)
5	200	L_{ox-t} and L_{ox-T} ($\gg 1$ μm)
5	300	$L_{ox-t} \gg L_{ox-T}$ ($\gg 1$ μm)
12	55	S + F
12	110	L_{ox-t} and L_{ox-T} ($\gg 1$ μm)
12	200	L_{ox-t} and L_{ox-T} ($\gg 1$ μm)
20	110	$L_{ox-T} \gg L_{ox-t}$ ($\cong 1$ μm)
20	200	$L_{ox-T} \gg L_{ox-t}$ ($\cong 1$ μm)

(b) Mixture of Gases with Less than 1% H_2 in the Overall Gas Mixture

P_{H_2O} (Torr)	flow 1% H_2 (cm^3 min^{-1})	flow N_2 (cm^3 min^{-1})	F_{tot} (cm^3 min^{-1})	F_{H_2} (cm^3 min^{-1})	% $H_2 = F_{H_2}/F_{tot}$	morphology of the particles
12	110	100	210	1.1	0.52	L_{ox-t} and L_{ox-T} ($\gg 1$ μm)
12	200	100	300	2	0.73	$L_{ox-T} \gg L_{ox-t}$ ($\cong 1$ μm)
12	200	50	250	2	0.88	L_{ox-t} and L_{ox-T} ($\gg 1$ μm)
12	200	20	220	2	1	L_{ox-t} and L_{ox-T} ($\gg 1$ μm)
12	100	200	300	1	0.33	L_{ox-t} and L_{ox-T} ($\gg 1$ μm)
12	50	200	250	0.5	0.2	$L_{ox-T} \gg L_{ox-t}$ ($\cong 1$ μm)

[a] L_{Ox-T} denotes long oxide whiskers, which are thick (D up to 100 nm). L_{Ox-t} denotes long oxide whiskers, which are thin ($D \cong 10-20$ nm). S denotes spherical particles. F denotes faceted particles.

increased to 1% (stage II). It was believed that the separation between the two reactions, i.e., formation of the needlelike germs in the first place and their subsequent growth, would afford a better control of the process, enabling more uniform whiskers to be derived.

Experiments were performed with the three types of particles synthesized in stage I by evaporation at $P_{H_2O} = 5$, 12 and 20 Torr. The results are summarized in Table 3a. The first point to emphasize is that the two sets of short needlelike particles (evaporated at $P_{H_2O} = 12$ and 20 Torr) in contact with the gas mixture (1% H_2/99% N_2) are transformed into long tungsten oxide nanowhiskers (several microns in length) at 840 °C. This is quite a large elongation considering the fact that the starting material consists of oxide needles usually no longer than 50 nm. Moreover, the amorphous oxide nanoparticles, which are shapeless ($P_{H_2O} = 5$ Torr), convert also into very long whiskers. Consequently, the starting needlelike morphology is apparently not relevant for inducing the growth of very long oxide whiskers during the annealing (stage II). Indeed, the trend could be described as follows: the lesser is the crystallinity of the precursor (tungsten suboxide) particles, the thinner and longer are the microlength oxide nanowhiskers obtained after stage II annealing. The most likely explanation for this observation would be that a sublimation of a part of the tungsten suboxide particles is followed by a transport of the clusters in the gas and their condensation on some other tungsten suboxide particles, which did not sublime. For example, amorphous nanoparticles smaller than say 5 nm are likely to be more volatile than the larger nanoparticles (Ostwald ripening). This point will be discussed in greater detail in the following section.

The second point to underline is the influence of the gas flow-rate (F) on the morphology of the particles, which is equivalent to a change in the pressure, (especially the partial pressure of hydrogen). This is particularly well illustrated in the series of measurements done with the particles synthesized at $P_{H_2O} =$ 12 Torr. In that case, a low flow-rate (55 cm^3 min^{-1}) generates spherical particles while a higher one (≥ 110 cm^3 min^{-1}) brings about the growth of long nanowhiskers. The trend is the same whatever the starting tungsten suboxide precursor. The flow-rate also influences the thickness of the particles, as shown by the experiment performed with the precursor synthesized at $P_{H_2O} = 5$ Torr. Indeed, in the particular case, where the limit of the flow-rate allowed by the equipment was reached (300 cm^3 min^{-1}), a majority of thin oxide nanowhiskers (10−20 nm in diameter) were observed instead of the usual mixture of thin and thick nanowhiskers (diameters up to 100 nm).

Since the amount of the starting oxide whiskers used for each experiment was quite similar from one batch to another ($\cong$5 mg), the differences observed by changing the flow-rates could be attributed to either of two parameters: the partial flow-rate of hydrogen in the reactor (partial pressure of hydrogen) or the total gas flow-rate (total pressure). This point is particularly well expressed by the experiment performed with the particles synthesized at $P_{H_2O} = 12$ Torr (stage I) and fired under a gas flow-rate of 55 cm^3 min^{-1} (stage II). In that case, whatever the fomation mechanism, the flow is so slow that spherical or faceted nanoparticles are formed. Even the original needlelike morphology is not preserved in such circumstances. Note also that the gas flow-rate may influence the apparent temperature of the gas mixture.

Consequently, the higher the flow-rate, the higher the driving force to generate long and thin oxide nanowhiskers.

The morphology of the oxide whiskers obtained after annealing the particles evaporated at $P_{H_2O} = 20$ Torr is different from the previous results, since the length and the thickness appear to be systematically limited to approximately 1 μm and 50−100 nm, respectively. These results indicate that, in such a case, the initial thickness of the needlelike nanoparticles dictates the final thickness of the elongated nanowhisker after annealing. Particular regard should be paid to the apex of these whiskers as they routinely formed perfect 90° heads following annealing. This head morphology excludes a vapor−liquid−solid (VLS) growth mode as a plausible growth mechanism.

III.1.d. Influence of the Hydrogen Concentration on the Elongation Process. This point was tested by varying the hydrogen concentration in the gas mixture. Indeed, by adding extra N_2 gas, the hydrogen concentration was diluted from 1% to approximately 0.2%, keeping the total flow-rate constant. The annealing experiments (stage II) were performed with the precursor synthesized at $P_{H_2O} = 12$ Torr (stage I). These results are collected in Table 3b.

The first noticeable observation is that the morphology of the resultant particles of two different batches annealed at the same total flow-rate (F_{Tot}) but with a different partial flow-rate

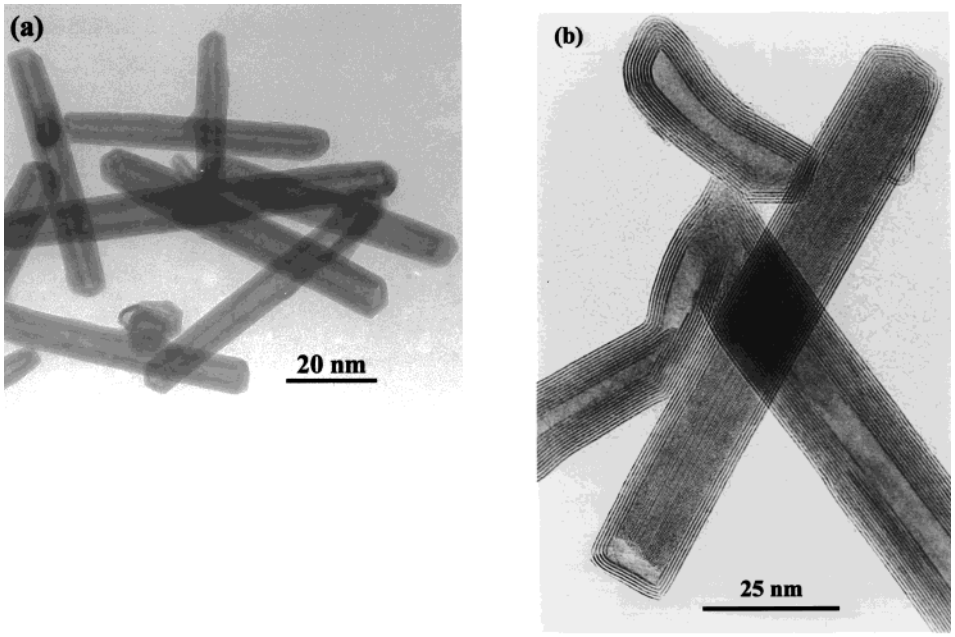

Figure 3. TEM micrographs of (a) a typical bundle of short WS_2 nanotubes and (b) a short WS_2 nanotube with oxide in the core.

of H_2 (F_{H_2}), is different. In parallel, for two experiments in which annealing was done with the same value of F_{H_2} but with two different values of the total flow-rate (i.e. by varying the nitrogen gas flow-rate), a slight morphological difference was observed. It is evident that both parameters (F_{H_2} and F_{Tot}) influence the morphology of the particles (stage II), as it was previously found for the case of the tungsten filament evaporated in contact with water vapor in the chamber (stage I).

Besides this consideration, it is important to note that this set of experiments was also a useful means of determining the minimum concentration of hydrogen required for providing the elongation of the whiskers. Globally, it appears that decreasing the concentration of hydrogen to 0.2% did not change drastically the morphology of the particles, which consists of long oxide whiskers >1 μm (Table 3b). It is noteworthy to underline the fact that the hydrogen concentration should be adjusted for the given amount of WO_{3-x} particles. Indeed, the ratio between the quantities of hydrogen and the starting WO_{3-x} powder must be kept constant to get the same kind of morphology during the annealing (stage II).

From this last experiment it emerges that a low concentration of hydrogen (0.2%) is sufficient for inducing the elongation process of the oxide whiskers. Furthermore, it suggests that the sublimed phase involved in the process has a stoichiometry very close to that of the starting precursor ($WO_{2.9}$).

As a conclusion of this first section, two key parameters for inducing the whisker's growth could therefore be discerned during stage II annealing: *the total gas flow (P_{Tot}) and the partial flow of hydrogen (P_{H2})*. These two factors will probably be involved in the synthesis of the WS_2 nanotubes as well, starting from the short WO_{3-x} whiskers.[12]

III.2. Synthesis of WS_2 Nanotubes (Stage III) from the WO_{3-x} Particles Produced by Evaporation in Stage I. The main process of the WS_2 nanotubes synthesis consists of sulfidizing the tungsten suboxide powder in a gas mixture which is composed of H_2/N_2 and H_2S, where H_2 plays the role of the reducer and H_2S the sulfidizing agent (eq 5, stage III).

$$WO_{3-x} + (1-x)H_2 + 2H_2S \rightarrow WS_2 + (3-x)H_2O \quad (5)$$

At the atomic scale, the process could be described as the creation of oxygen vacancies in the oxide structure followed by insertion of sulfur atoms to the vacant positions.[13] Since the growth process of the sulfide proceeds from outside in, sulfur atoms have to cross the already existing compact layers of sulfide and therefore the oxide to sulfide conversion is diffusion controlled. In this way, after a few hours of reaction all the W−O bonds of the starting material are converted into W−S bonds, leading to hollow structures without a substantial morphological change. Furthermore, since the densities of WO_3 ($\rho = 7.16$ g·cm^{-3}) and WS_2 ($\rho = 7.5$ g·cm^{-3}) are quite similar,[16] the original structure of WO_3 (and therefore WO_{3-x}) is preserved throughout the reaction as was the case for the IF nanoparticles starting with quasispherical particles of WO_3.[12] The formation of completely closed nanotubes is therefore consistent with the results of the previous study.

Considering the fact that homogeneous phases of either short needlelike (stage I) or long whiskers (stages I + II) of tungsten suboxide could be produced, experiments with the two types of precursors have been undertaken.

III.2.a. Synthesis of WS_2 Nanotubes Starting from the Short Whisker Precursor (Stages I + III). Short WO_{3-x} needlelike particles, produced by evaporation at $P_{H_2O} = 12$ Torr in stage I, were placed in a reducing/sulfidizing atmosphere as described previously. To understand which factors are responsible for the morphology of the converted sulfidized samples, only one parameter among three was changed at a time: the flow-rates of H_2/N_2, H_2S, and the hydrogen concentration in the gas mixture. In all these experiments the temperature was maintained at 840 °C. The data from these experiments are summarized in Table 4. Each section of the table (4a, 4b, and 4c) contains experiments in which one parameter was changed at a time. Comparisons could therefore be done inside each set of experiments and between them.

When a gas mixture with 5% hydrogen was used (Table 4a), most of the needle batches had similar morphologies irrespective of the flow-rate ratio ($F_{H_2/N_2}/F_{H_2S}$). A TEM picture of a typical bundle of short nanotubes stemming from those batches is presented in Figure 3. The particles are hollow and the WS_2 layers contain very few defects. The apexes of the tubes are

Table 4. Influence of the Flow-Rate of the Gases and the Ratio between Them on the Morphology of the Sulfidized Samples for Different Concentrations of Hydrogen in the Gas Mixture[a]

(a) 5%H_2/95% N_2

flow of 5%H_2/ 95% N_2 (cm^3 min^{-1})	flow of H_2S (cm^3 min^{-1})	F_{H_2}/F_{H_2S}	$F_{H_2/N_2}/F_{H_2S}$	morphology of the samples
110	4	1.375	27.5	Sh
110	2	2.75	55	Sh
110	1	5.5	110	Sh
110	0.5	11	220	Sh with W inside
110	0*			L_T with W inside + W
200	2	5.5	110	Sh
200	1	10	200	Sh with W inside
200	0.5	20	400	(L_t and L_T + Sh) with W inside
55	2	1.375	27.5	Sh

(b) 1% H_2/99% N_2

flow of 1%H_2/ 99% N_2 (cm^3 min^{-1})	flow of H_2S (cm^3 min^{-1})	F_{H_2}/F_{H_2S} (cm^3 min^{-1})	$F_{H_2/N_2}/F_{H_2S}$	morphology of the samples
110	2	0.55	55	Sh + 2H−WS_2
110	1	1.1	110	Sh + L_t and L_T + IF + 2H−WS_2
110	0.5	2.2	220	Sh
110	0.3	3.7	314	nondefined shape + IF + Sh
200	2	1	100	bad encapsulation
200	1	2	200	Sh + very few L + IF + 2H-WS2
200	0.5	4	400	(Sh + L_t and L_T + IF) with W inside
55	2	0.275	27.5	2H-WS_2

(c) Less than 1% H_2/99% N_2

flow of 1%H_2/ 99% N_2 (cm^3 min^{-1})	flow of N_2 (cm^3 min^{-1})	flow of H_2S (cm^3 min^{-1})	F_{H_2}/F_{H_2S}	% $H_2 = F_{H_2}/F_{tot}$	morphology of the samples
200	100	1	2	0.66	Sh + L_t
110	100	1	1.1	0.52	Sh + L_t
100	200	1	1	0.33	Sh with W inside + L_t and L_T
50	200	1	0.5	0.2	Sh + L_t
100	200	0.5	2	0.33	(Sh+ L_t and L_T) with W inside
110	100	0.5	2.2	0.52	L_T and L_t + Sh
200	100	0.5	4	0.66	L_T and L_t ≫ Sh with W inside
200	100	2	1	0.66	L_t and L_T ≫ Sh
110	100	2	0.55	0.52	Sh ≫ 2H−WS_2

[a] All measurements have been done with the starting WO_{3-x} precursor produced at $P_{H_2O} = 12$ Torr. Sh and L denote short and long nanotubes, respectively. L_T denotes long and thick nanotubes and L_t denotes long and thin nanotubes. An asterisk indicates the synthesis was done without addition of H_2S but with residual sulfur from the previous synthesis.

quite perfectly closed. The length of the nanotubes is approximately the same as those of the starting WO_{3-x} precursors (50 nm in length and 15 nm in diameter). In contrast, when the ratio F_{H_2}/F_{H_2S} was very high, long nanotubes of several microns in length could be discerned in the samples among bundles of short nanotubes. However, the formation of long nanotubes was always accompanied by the presence of metallic tungsten in their cores (Figure 4) and, in several cases, spherical nanoparticles of tungsten were found. Also, the number of WS_2 layers was rather small in this case. This is attributed to fast reduction of the tungsten oxide core to the pure metal and subsequently to the slow diffusion of sulfur through the compact metallic core.[10] Furthermore, a wide size-distribution among the long nanotubes was found. Indeed, in such conditions, two types of nanotubes were present: "thin nanotubes", with a typical diameter of about 20 nm, and "thick" ones, which could reach a diameter up to 100 nm.

The variety of morphologies which appear by varying the flow-rate of forming gas (H_2/N_2) and H_2S shows that the ratio between the two gases is essential for determining the final shape of the sulfidized nanotubes.

More precisely, when the ratio F_{H_2}/F_{H_2S} exceeds the value of ca. 10, either tungsten particles or nanotubes containing a tungsten core start to appear. In that case, the hydrogen concentration in the reactor is so high compared with that of sulfur (for the amount of precursor taken) that the tungsten

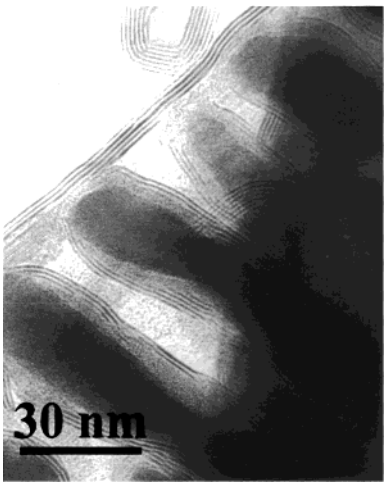

Figure 4. TEM micrographs of a WS_2 nanotube with tungsten metal inside the core.

suboxide particles (WO_{3-x}) are reduced almost instantaneously into W. This is another manifestation of the competition which occurs between the reduction and the sulfidization processes. *To avoid such an unwieldy situation, one has to operate in a specific ratio with $F_{H_2}/F_{H_2S} < 10$.* When the concentration of H_2 in the forming gas was about 5%, short nanotubes were

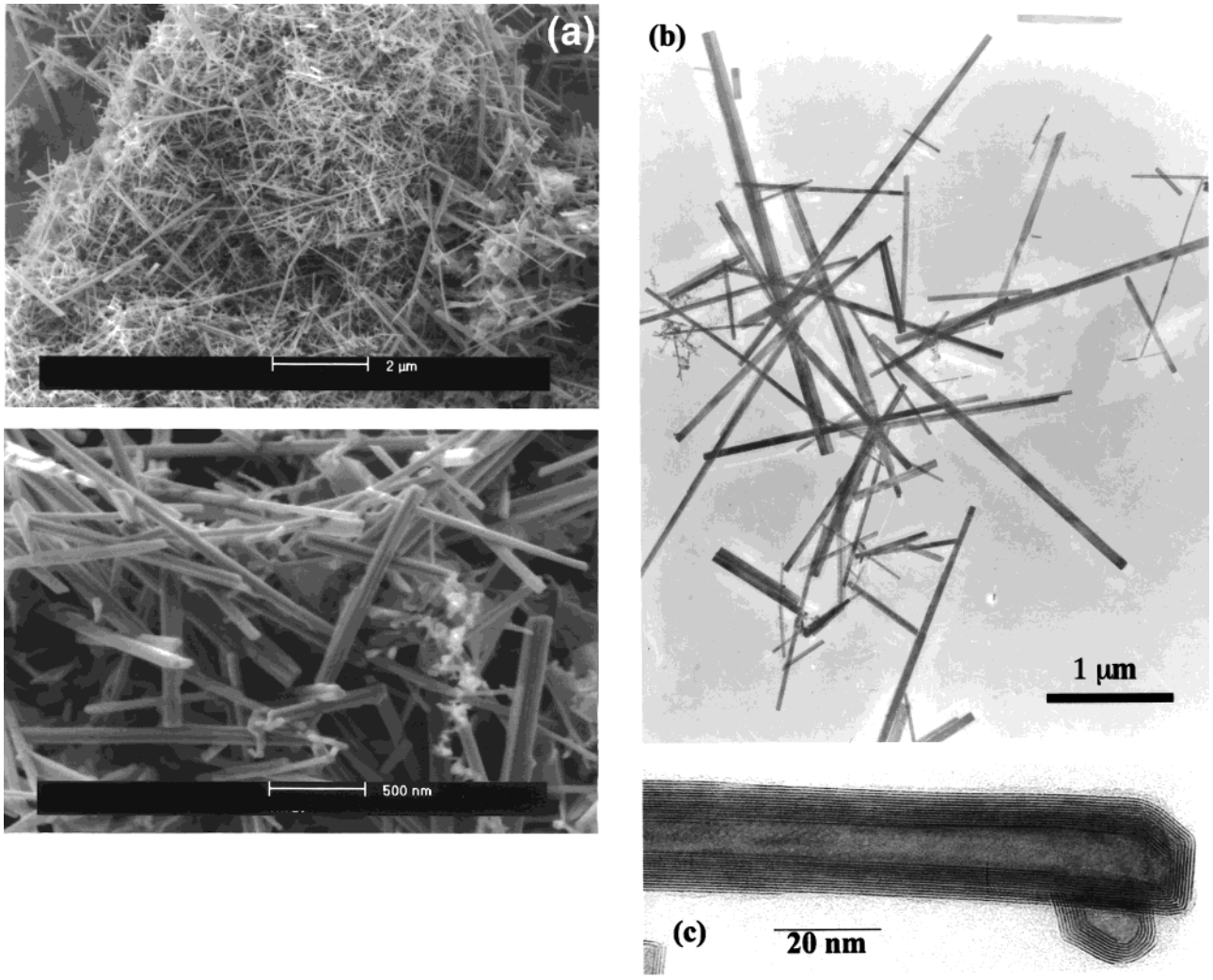

Figure 5. (a) SEM micrograph of a bundle of long WS_2 nanotubes at two different magnifications, (b) TEM micrograph of a bundle of long WS_2 nanotubes, and (c) enlargment of one hollow WS_2 nanotube from this bundle.

produced in the range $1.4 \leq F_{H_2}/F_{H_2S} \leq 11$ and long ones were observed for a ratio F_{H_2}/F_{H_2S} above 11.

Another aspect for the influence of the flow-rate ratio F_{H_2}/F_{H_2S} on the nanotubes morphology is illustrated in the experiments where no H_2S was added to the system at all. In this case, the reactor was not flushed with N_2 prior to the experiment. Here traces of sulfur, which remained on the reactor walls from the previous experiment, led to the formation of long nanotubes (Table 4a). This point emphasizes the fact that the ratio F_{H_2}/F_{H_2S} is essential for the final morphology of the sulfidized particles.

When the hydrogen concentration in the forming gas was lowered to 1% instead of 5%, the factor F_{H_2}/F_{H_2S} appeared not to be the only one responsible for the morphological changes. Indeed, two different batches, for which the ratio F_{H_2}/F_{H_2S} was kept constant (Table 4b: batches 3 and 6), gave two discernible morphologies. Besides that, careful examination of the data revealed that, decreasing the hydrogen concentration in the gas mixture leads frequently to the formation of long nanotubes instead of the usual short ones. This trend was even more pronounced in experiments performed with an extremely low hydrogen concentration (less than 1%, see Table 4c). As a matter of fact, all the batches performed with hydrogen concentration below 1% led to the growth of either a mixture of short and long nanotubes or to almost pure phases of long nanotubes (see Figure 5). The results of Table 4 lead to the conclusion that the appearance of long nanotubes depends on the ratio between the flow-rate of hydrogen and the total flow-rate of gases (F_{H_2}/F_{Tot}).

It emerges therefore, that to achieve the formation of long nanotubes, two flow-rate ratios have to be carefully controlled: F_{H_2}/F_{H_2S} and F_{H_2}/F_{Tot}. The conditions required for providing long nanotubes as a majority phase in a reproducible manner are consequently the following:

$$0.5 \leq F_{H_2}/F_{H_2S} \leq 4.5 \text{ and } 0.002 \leq F_{H_2}/F_{Tot} \leq 0.007$$

To obtain homogeneous phases consisting of purely long nanotubes without tungsten in their core, the conditions are even more restrictive:

$$1 \leq F_{H_2}/F_{H_2S} \leq 2.2 \text{ and } 0.005 \leq F_{H_2}/F_{Tot} \leq 0.007$$

It emerges from all these results that a careful control of the synthesis parameters leads to a specific and desireable morphology of the nanotubes.

III.2.b. Synthesis of WS_2 Nanotubes Starting with the Microlength Oxide Whiskers (Stages I + II + III). The purpose of this last study was to explore the possibility of synthesizing long WS_2 nanotubes from the already exisiting long oxide nanowhiskers obtained in stage II. The long oxide nanowhiskers synthesized from the short whiskers (see section III.1)

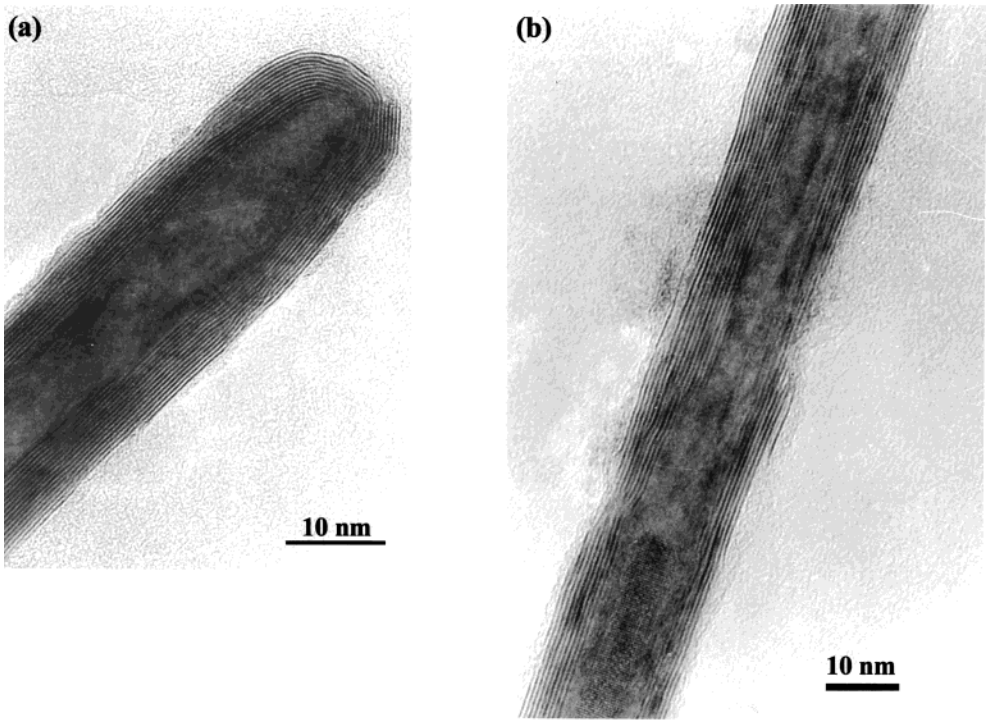

Figure 6. TEM micrographs of (a) the apex of one WS_2 nanotube synthesized by the "two step method" (stage I + II + III) and (b) nanotube walls, which contain several defects.

were placed in a reducing and sulfidizing atmosphere without taking specific attention to the ratios F_{H_2}/F_{H_2S} and F_{H_2}/F_{Tot}. All attempts led to the formation of long nanotubes, although the degree of crystallinity of the nanotubes was not perfect. The WS_2 layers contained plenty of defects and a rather large proportion of the nanotubes were not totally closed at their apex (Figure 6).

In comparing the two methods, it is evident that, although the first method (i.e. starting from short whiskers, stages I + III) is more difficult to control, it gives more satisfactory results, notwithstanding the fact that the second method (i.e. stages I + II + III) could probably be further optimized. However, as opposed to the first method, the latter method lends itself to the synthesis of nanotubes from related compounds, such as WSe_2 or mixed WS_2/WSe_2, using prepared long oxide nanowhiskers as a precursor, a direction that is currently being investigated. Indeed, WSe_2 nanotubes were prepared by heating a selenium ingot at 350 °C downstream of the main reactor, which was heated to 760 °C. Forming gas (1% H_2/99% N_2, 110 cm^3 min^{-1}) was provided in this case. The resulting WSe_2 nanotubes were quite perfect in shape, but many of them did not have closed ends.

IV. Discussion

From the results described previously (section III.2), two kinds of processes could be distinguished: the first one that leads to the formation of short nanotubes having approximately the same size as their precursors and the other that ends with a pure phase of long nanotubes several microns in length. The fact that the long WS_2 nanotubes could be produced starting from short WO_{3-x} precursors raises the question of the origin of such an elongation.

The production of tungsten oxide whiskers by various methods has been reported already.[17,18] One example among them concerns the growth of $WO_{2.72}$ ($W_{18}O_{49}$) whiskers by resistive heating of a tungsten foil within the TEM[17] (i.e. a reducing atmosphere). Preheating the tungsten foil in air at 500 °C, which formed a top oxide film, was found to enhance the needle growth. The elongation rate was observed to be inversely proportional to the whisker radius, which favored the growth of thin (30 nm) nanowhiskers. The growth of the nanowhiskers was attributed to the evaporation of the oxide and its subsequent condensation. It was further shown that reduction of a WO_3 powder by annealing in H_2 gas leads to the formation of $WO_{2.72}$ needles by a process described as an evaporation−condensation process.[18] The $W_{18}O_{49}$ phase consists of pentagonal columns,[19] which promotes asymmetric growth along the column axis ($||c$), thus favoring whisker growth. The vapor pressure of WO_3 at the prevalent temperatures is about 10^{-7} Torr,[20] and the various suboxides were found to be appreciably less volatile. Polymeric clusters of the form $(WO_3)_n$ ($n = 3$ to 5) were identified in the gas phase of a heated WO_3 powder.[21] Of this series, the $n = 3$ cluster was by far the most abundant. These results are consistent with the study of Ackermann et al.,[22] who reported the formation of $(WO_3)_n$ clusters with a larger range of n ($n = 1$ to 5) compared to the previous work but with $n = 3$ as the predominant phase as well.

It was also shown that water vapor enhances the rate of WO_3 evaporation[18,23] and that hydrated clusters of the form $WO_{3-x}{\cdot}nH_2O$, which are volatile, promote the growth rate of WO_{3-x} needles (whiskers). These clusters are being formed

(17) (a) Hashimoto, H.; Tanaka, K.; Toda, E. *J. Phys. Soc. Jpn*. **1960**, *15*, 1006. (b) Hashimoto, H.; Kumao, A.; Eto, T.; Fujiwara K. *J. Cryst. Growth* **1970**, *7*, 113.

(18) Sarin, V. K. *J. Mater. Sci*. **1975**, *10*, 593.

(19) (a) Magneli, A. *Ark Kemi* **1950**, *1*, 223. (b) Sahle, W. *J. Solid State Chem.* **1982**, *45*, 324. (c) Sahle, W. *J. Solid State Chem.* **1982**, *45*, 334.

(20) According to *Gmelins Handbuch der Anorganischen Chemie* (Meyer, R. J., Ed.; Verlag Chemie: Berlin 1933; Vol. 54, p 122), the vapor pressure of WO_3 is 1 Torr at this temperature. However, a calculation based on more recent data in *The Oxide Handbook*, 2nd ed. (Samsonov, J. V.; IFI/Plenum Data Company, 1982; p 156) yield a vapor pressure of 10^{-7} Torr.

(21) Berkowitz, J.; Chupka, W. A.; Inghram, M. G. *J. Chem. Phys*. **1957**, *27*, 85.

(22) Ackermann, R. J.; Rauh, E. G. *J. Phys. Chem.* **1963**, *67*, 2596.

(23) Millner, T.; Neugebauer, J. *Nature* **1949**, *163*, 602.

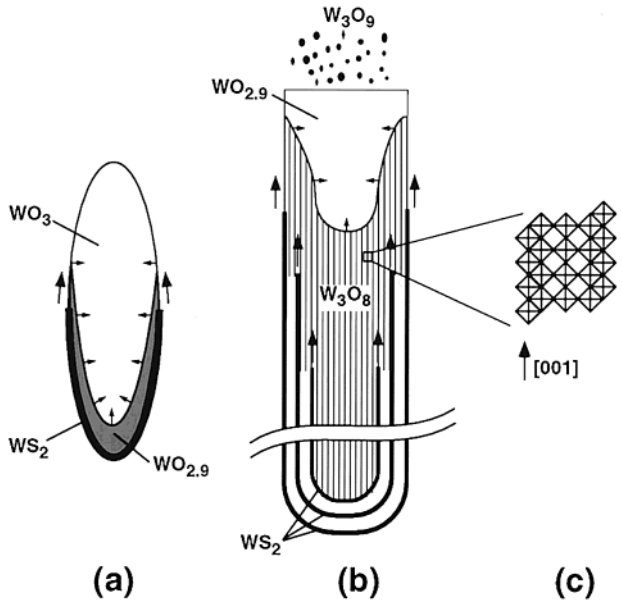

Figure 7. Schematic illustration of the growth process of the encapsulated sulfide/oxide nanowhisker; (a) initialization of the sulfidization process of the asymmetric oxide nanoparticle; (b) growth of a long sulfide/oxide encapsulated nanowhisker; and (c) enlargment of the $\{001\}_R$ CS planes exhibiting within one CS plane regions of edge-sharing octahedra.

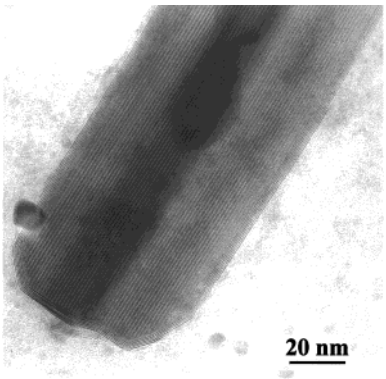

Figure 8. TEM micrograph of one part of a WS_2 nanotube in an intermediate stage where tungsten suboxide is in the core. The core presents ordered $\{001\}_R$ CS planes[15,25] along the tube axis. The stoichiometry of this sample phase belongs to the homologous series W_nO_{3n-1} (W_5O_{14}).

spontaneously during the reduction of WO_3 powder by H_2 gas at elevated temperatures.[18]

One can visualize the growth mechanism of the long nanotubes (stages I + III) as follows. At the first instant of the reaction (Figure 7a), the needlelike oxide nanoparticle reacts with H_2S and forms a protective tungsten disulfide monomolecular layer, prohibiting coalescence of this nanoparticle with neighboring oxide nanoparticles, which are themselves coated with a protective monolayer of WS_2. Due to the fast whisker growth mode, the whisker tips remains uncovered. Simultaneous condensation of $(WO_3)_n$ or $(WO_{3-x}{\cdot}H_2O)_n$ clusters on the uncovered (sulfur-free) nanowhisker tip and subsequent reduction by hydrogen gas leads to continuous growth of the sulfide-coated oxide nanowhiskers. This process is schematically illustrated in Figure 7b. A plausible explanation for the uniaxial growth mode of the oxide nanowhisker is that during the reaction, a slow sublimation of a fraction of the tungsten suboxide powder takes place, a phenomenon already indicated for the growth of WO_{3-x} whiskers (section III.1). Here, small oxide nanoparticles (<5 nm), which are likely to be less stable than their larger counterparts,[24] are prone to rapid vaporization and therefore provide the necessary tungsten-oxide rich gaseous phase.

The structural aspects of the reduction/sulfidization of tungsten-oxide nanoparticles has been studied in some detail, recently.[15] It was found that hydrogen diffusion through various crystal faces produces a multidomain CS structure in the quasispherical nanoparticles. On the other hand, the same diffusion process and reduction proceeds in a distinctly different way in the asymmetric oxide nanowhiskers. Here, diffusion occurs mainly along the growth (long) axis of the nanowhisker, and consequently the sulfide layer grows parallel to an exposed ReO_3-type oxide surface, presumably containing some partially reduced sites. Ordering of shear planes within the resultant oxide encapsulate may occur either concurrently or just prior to sulfidization to form one of a number of possible lamellar oxide phases, for example W_3O_8.[15,25−27]

This phase provides a sufficiently open structure for the sulfidization to proceed until the entire oxide core is consumed. Complete conversion of this highly ordered oxide by sulfide leads to the formation of hollow WS_2 nanotubes, which are quite perfect in shape and are (almost) free of dislocations. Further reduction of the oxide core would bring the sulfidization reaction into a halt.[10] Indeed, in the absence of H_2S, the tungsten oxide nanowhiskers are rapidly reduced into pure W metal under similar conditions. Therefore, the sulfide encapsulation of the oxide nanowhisker, which tames the reduction of the inner oxide core and preserves its open structure, allows for the gradual conversion of this nanoparticle into a hollow WS_2 nanotube. The penetration of the sulfur atoms through the compact outer tungsten sulfide layer is diffusion controlled and consequently this process is rather long (ca. 2 h depending on the conditions of the reaction).

Some remarks and questions which remain open for further research must, however, be added. First, no assignment of the volatile oxide phase could be done in this study. As a matter of fact, the volatility of the tungsten suboxide has been studied already,[17,18,20−23] but no data are available concerning the stoichiometry of the volatile oxide phase, which would have been formed in conditions similar to the present experiments. Moreover, assuming that some of the volatile oxide will be deposited elsewhere, one could anticipate finding a blue oxide powder or tungsten disulfide on the walls of the reactor or in the gas exhaust. One explanation to the absence of both is that a noncolored volatile phase $WO_{3-x}{\cdot}nH_2O$ ($x = 2$ to 3) has been formed and lands on cold zones where the rate of the reaction with H_2S is too slow to be recognized. It is more likely, however, that the deposition of the tungsten-oxide clusters on the oxide tip resembles the often encountered catalytic vapor−liquid−solid growth mode.[17b] Here, a strong thermodynamic driving force eliminates any side reaction, leaving a pure phase of whiskers. Note also that the growth of pure WO_{3-x} nanowhisker phases was reported in the past.[17,18,21−23] Figure 8 shows the head of a long oxide nanowhisker capped by a few tungsten sulfide layers and ordered CS structure in the core.

With regard to the elongation of the tungsten suboxide whiskers, it is important to emphasize that long oxide nano-

(24) Goldstein, A. N.; Echer, C. M.; Alivisatos, A. P. *Science* **1992**, *256*, 1425.
(25) Miyano, T.; Iwanishi, M.; Kaito, C.; Shiojiri, M. *Jpn. J. Appl. Phys.* **1983**, *22*, 863.
(26) Rothschild, A.; Frey, G. L.; Sloan, J.; Tenne, R. Manuscript in preparation.
(27) Iguchi, E. *J. Solid State Chem.* **1978**, *23*, 231.

whiskers were obtained also starting from amorphous tungsten-oxide material (stages I + II). This observation shows that even without a set of needlelike particles, a complete ordered stacking is achieved. This result counterbalances the intuitive notion that a needlelike morphology is necessary for generating the elongation process. It is not unlikely, however, that at the first instant of the annealing process, the amorphous material develops into needlelike formations.

Another puzzle in the proposed mechanism for the elongation of the nanowhiskers and their conversion into sulfide nanotubes is the postulated stability of the metal-oxide clusters in the gas phase against reaction with H_2S gas. This inertness could perhaps be attributed to the stable hexagonal rings formed by $(MO_3)_3$ clusters.[28]

Finally, it was observed that starting with long oxide whiskers did not always lead to perfectly closed WS_2 nanotubes. This situation was more pronounced when selenization was used in place of sulfidization. In the case of selenization, even the thin nanotubes were produced with open caps.

One explanation for this phenomenon could be related to the activation energy required for breaking the W−O bonds. This energy is probably higher in the case of the "two step method", when long and crystalline whiskers are used as compared to the "one step method" (where short semicrystalline needlelike particles are used). In the latter case, the sulfidization occurs concomitantly with the reduction, thereby blocking the relaxation phenomenon of the W−O bonds and enabling their rapid conversion into W−S bonds. It is noticeable that in the "two step method" (stage I + II + III), the reduction of the whiskers occurs already during the second stage, leading often to the formation of long reduced oxide whiskers with CS planes in their core.[26] Once these CS planes are present in the structure, the conversion of the W−O to W−S bonds, during stage III, requires more energy, since the structure is more highly ordered and compact.

V. Conclusions

Two objectives were realized in this study. First, the problem of the reproducibility of the WS_2 nanotubes synthesis has been resolved. Indeed, in the past, the formation of WS_2 nanotubes was very uncontrolled and not particularly reproducible. By determining the role of each experimental parameter separately, the conditions for obtaining, reproducibly, unique phases of WS_2 nanotubes (either short or long) have been determined. Second, an analysis of all the results has led to a plausible mechanism for explaining the growth mechanism of the whiskers and formation of the resulting encapsulates.

The use of the current nanotubes as tips for scanning probe microscopy has been recently accomplished.[29] These tips could be used for numerous applications, such as imaging rough surfaces having features with high aspect ratio. The robustness and inertness of these tips is rather promising for, e.g., imaging of biologically significant systems.

Acknowledgment. We thank Mrs. Tatiana Tsirlina for the assistance with the WSe_2 nanotube synthesis. We also thank Mr. Van der Wal from Philips Electron Optics B.V. (Eindhoven) for the SEM pictures taken on the XL30-ESEM FEG instrument. This research was partially supported by grants from the Israeli Ministry of Science (Tashtiot program), the Levine Foundation of the Weizmann Institute, and the G.M.J. Schmidt Minerva Center.

JA994118V

(28) Berkowitz, J.; Inghram, M. G.; Chupka, W. A. *J. Chem. Phys.* **1957**, *26,* 842.

(29) Rothschild, A.; Cohen, S. R.; Tenne, R. *Appl. Phys. Lett.* **1999**, *75*, 4025.